CHEMISTRY OF MATERIALS
Cite This: Chem. Mater. 2019, 31, 8639–8648
Article
pubs.acs.org/cm

Effect of Copper Substrate Surface Orientation on the Reductive Functionalization of Graphene

Xu Zhang,*[,†,#] Da Luo,[†] Hanyang Zhang,[†] Dae Yeon Hwang,[‡] Sung O. Park,[‡] Bao-Wen Li,[†] Mandakini Biswal,[†] Yi Jiang,[†] Yuan Huang,[†] Sang Kyu Kwak,[†,‡,⊥] Christopher W. Bielawski,*[,†,§,⊥] and Rodney S. Ruoff*[,†,‡,§,∥]

[†]Center for Multidimensional Carbon Materials (CMCM), Institute for Basic Science (IBS), Ulsan 44919, Republic of Korea
[‡]School of Energy and Chemical Engineering, [§]Department of Chemistry, [∥]School of Materials Science and Engineering, and [⊥]Department of Energy Engineering, Ulsan National Institute of Science and Technology (UNIST), Ulsan 44919, Republic of Korea

Supporting Information

ABSTRACT: Although substrate composition can influence the chemical reactivity of graphene, substrate lattice orientation provides a valuable alternative. The effect of Cu surface orientation on the reactivity of graphene was explored through a reductive transformation. Among the substrates tested, only Cu(111) led to the efficient, fast and uniform functionalization of graphene, as demonstrated by Raman mapping, and this arose from compressive strain induced by Cu(111). Functionalization effectively relaxes the strain, which can be subsequently reintroduced after thermal treatment. Theoretical calculations showed how compression facilitates the reduction and hybridization of carbon atoms, while coupling experiments revealed how kinetics may be used to control the reaction. The number of graphene layers and their stacking modes were also found to be important factors. In a broader context, a description of how graphene undergoes chemical modification when positioned on certain metal substrates is provided.

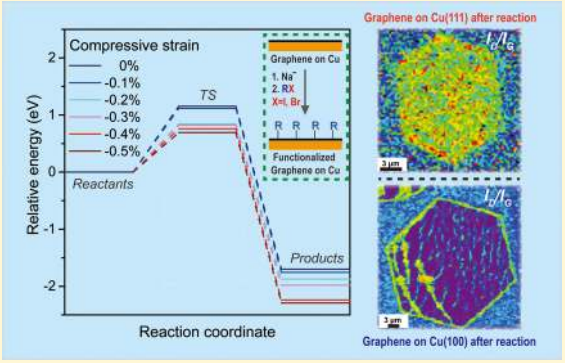

INTRODUCTION

Chemical functionalization is a process that can be used to tailor the structure and properties of graphene.[1−3] A variety of methodologies have been used to graft functional groups onto graphene, including diazo-coupling,[4−11] cycloaddition,[12,13] photochemistry,[14,15] and reduction.[16−19] With regard to the controlled functionalization of defect-free graphene in certain transformations, several factors have been found to significantly alter the chemical reactivity, including the nature of the substrate,[6,18,20,21] tensile strain,[8,9] the number of layers (n),[5,18,19,22] and the stacking mode (when $n \geq 2$).[10,15] However, these findings were only acquired from graphene on dielectric or semiconductor substrates. In contrast, graphene and its functionalized derivatives on metals, particularly Cu, can be directly used in a variety of sensing and other applications. Compared with graphene on SiO_2/Si, graphene on Cu excludes the influence of polymer residues and trapped molecules, and thus provides a relatively clean surface for subsequent functionalization. Moreover, graphene on metals may provide platforms that enable one-sided functionalization and thus facilitate access to two-sided graphene that is functionalized in an asymmetric manner. However, graphene on Cu has only been discussed in gas- or solid-phase reactions,[23−25] and was reported to exhibit a significantly lower reactivity than graphene on SiO_2.[23,24] Since the surface orientations of common metal foils may be quite different, which can challenge systematic reactivity studies, understanding how the surface orientation of the metal substrate affects the chemistry of the overlying graphene is warranted.

Cu foils are widely used to grow graphene by chemical vapor deposition (CVD),[26,27] and graphene on Cu provides a convenient platform for functionalization. However, spatial inhomogeneities in the Cu substrate, including lattice (mis)-orientation of the grains, step bunching (i.e., groups of ripple-like, periodic Cu steps formed during the CVD growth of graphene),[28] grain boundaries and oxidation, and graphene status (e.g., wrinkles, grain boundaries, strain, and charge doping),[29,30] can lead to nonuniformity when attempting to covalently functionalize the graphene.[25] Relationships between the chemical reactivity and the local structure of graphene grown on Cu, which may be strongly influenced by the orientation of the Cu surface, have not been well investigated because of the limited availability of reproducible graphene samples grown on monocrystalline Cu foils with a controlled

Received: May 2, 2019
Revised: October 1, 2019
Published: October 17, 2019

DOI: 10.1021/acs.chemmater.9b01729
Chem. Mater. 2019, 31, 8639−8648

orientation. In this context, we recently reported that graphene grown epitaxially on a well-defined Cu(111) foil substrate is under compressive stress,[31] and found that there is only a very small rotation angle between the hexagonal graphene lattice and the hexagonal arrangement of Cu atoms on the Cu(111) surface. Such a small lattice rotation angle can be expected to produce a relatively large frictional force between the epitaxial graphene and the underlying Cu(111) foil substrate,[31] and thus may play a crucial role in maintaining the compressive strain in graphene when the Cu(111) foil contracts while cooling from the growth temperature of 1070 °C to room temperature. The epitaxial graphene shows a relatively uniform compressive strain of ~0.3%, and appears to be a wrinkle-free, single crystal. Since such samples should not contain grain boundaries or wrinkles, they can be expected to facilitate in-depth studies of graphene.

To efficiently functionalize both single-layer (1L) and bilayer (2L) graphene, a reductive reaction was conducted by treating graphene with a solution of $[K(15\text{-crown-}5)_2]Na$, followed by an aryl or alkyl halide.[19] While we previously noted that this approach efficiently functionalizes 1L graphene, where the graphene is epitaxial to the Cu(111) surface, the chemistry was not explored in detail.[31] Here, we describe how the surface orientation of the Cu influences the reaction of graphene. Spatially resolved Raman spectroscopy imaging was used to examine the reactivities of graphene grown on three Cu foil substrates: (i) Cu(111), (ii) a crystalline surface close to Cu(100) (termed Cu(100) for simplicity, Figure S1, Supporting Information (SI)), and (iii) a polycrystalline Cu foil. Faster and more homogeneous functionalization was found for graphene on Cu(111) than on Cu(100) or polycrystalline Cu, and was attributed to the larger compressive strain of graphene on Cu(111). It was found that functionalization and subsequent thermal treatment "relaxed" and reproduce the compressive strain in the graphene, respectively. Molecular dynamics (MD) and density functional theory (DFT) calculations were also used to understand the nature of the compression induced by the orientation of the Cu surface and its effect on the reactivity of graphene. The degree of the reaction was changed by varying temperature and time, and the reaction kinetics were obtained from such data. In addition, the reductive chemistry of 2L graphene on Cu(111) and the influence of graphene stacking were investigated to better understand how to control the functionalization of few-layer graphene samples.

RESULTS AND DISCUSSION

Functionalization of Graphene on Different Substrates. Our two-step reductive reaction involves the sequential treatment of graphene with an alkalide reductant in conjunction with aryl or alkyl halides.[19] Briefly, when mixing a sodium–potassium alloy (NaK, liquid, 1:1 atom ratio) and 15-crown-5 in anhydrous tetrahydrofuran (THF), 15-crown-5 coordinates with K^+ and facilitates the dissolution of NaK to produce a blue solution of $[K(15\text{-crown-}5)_2]Na$.[32,33] As shown in Figure 1a, graphene is reduced when exposed to the reductive sodide solution for a designated period of time (t_1). Next, an organohalide is introduced into the mixed solution to react for a time t_2. We found that varying t_1 significantly affected the degree of functionalization, whereas changing t_2 had a relatively limited effect.[19]

Three Cu foil substrates, namely, Cu(111), Cu(100), and polycrystalline Cu (*p*-Cu), were independently used in this study to explore the effect of crystalline orientation of the Cu substrate on the reactivity of graphene. Hexagonal or irregular graphene islands were grown by CVD on the three substrates (more information on the graphene islands is provided in the SI). Note that the single-crystal Cu(111) and Cu(100) substrates were obtained by our recently reported contact-free method,[34] and the graphene islands on Cu(111) appeared to be uniform in functionalization degree. The selected graphene islands/regions for Raman maps are representative of all graphene islands/regions on the same substrate. The surface orientations of the Cu foils underlying the graphene were measured by electron backscatter diffraction (EBSD) and the corresponding images are shown in Figure S2. Monolayer islands on Cu(111), Cu(100), or *p*-Cu were subjected to the conditions used to induce reductive functionalization.[19] For comparison, the same reaction was repeated on a continuous 1L graphene grown on polycrystalline Cu and transferred onto SiO_2 (300 nm)/Si. Since a graphene edge with a larger number of defects is more reactive than the basal plane,[5] the Raman spectra shown in Figure 1b–d are from the internal regions of the islands.

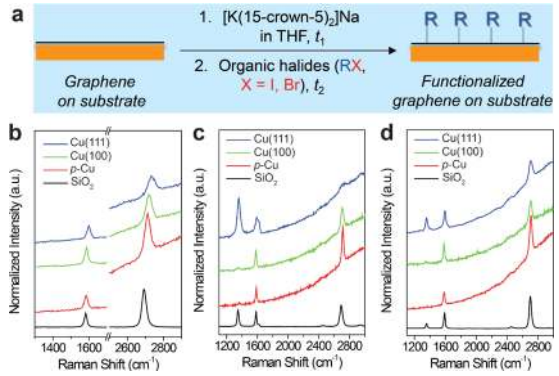

Figure 1. Summary of the reductive functionalization reaction used to modify graphene on various substrates (indicated) and the corresponding Raman data. (a) Reaction procedures of the two-step reductive functionalization. (b) Raman spectra recorded from 1L graphene islands on different substrates. (c) Raman spectra recorded from 1L islands after functionalization with iodobenzene. Reaction conditions: $[[K(15\text{-crown-}5)_2]Na]_0$ ($[C_{NaK}]_0$) = 0.02 M; t_1 = 5 min; t_2 = 5 min; and temperature (T) = 20 °C. (d) Raman spectra recorded from 1L islands after functionalization with bromobenzene. Reaction conditions: $[C_{NaK}]_0$ = 0.04 M; t_1 = 10 min; t_2 = 5 min; and T = 20 °C. Each spectrum was averaged from ten spectra recorded at different positions on each sample. λ_{laser} = 488 nm.

All four graphene samples showed no D peaks (Figure 1b), indicating they are of high quality with few defects. We found that 1L graphene on Cu(111) is noticeably different from those on Cu(100), *p*-Cu, or SiO_2 from the Raman G and 2D band frequencies (ω_G and ω_{2D}), as well as the full-width at half-maximum of the 2D peak ($FWHM_{2D}$) (Table S1). These differences can be attributed mainly to charge doping and mechanical strain,[29] and will be discussed below.

Raman spectroscopy can be used to assess the degree of covalent functionalization, more specifically, by measuring the ratio of the height of the defect-activated D peak (sp^3-defect for the covalent functionalized graphene) to the characteristic G peak (I_D/I_G).[35−38] Figure 1c shows the spectra acquired from the four graphenes exposed to a solution of $[K(15\text{-crown-}5)_2]Na$ for 5 min, followed by the dropwise addition of iodobenzene in THF and further immersion for 5 min. The

DOI: 10.1021/acs.chemmater.9b01729
Chem. Mater. 2019, 31, 8639−8648

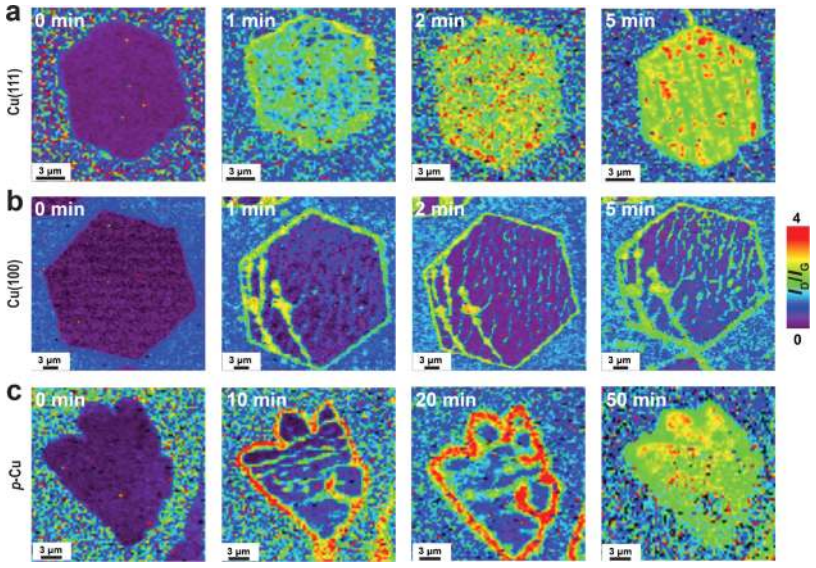

Figure 2. Progress of the reductive reaction on graphene islands as revealed by sequential Raman I_D/I_G (height) maps over time. (a) A 1L graphene island on Cu(111). (b) A 1L island on Cu(100). (c) A 1L island on *p*-Cu. The reaction time t_1 of each run is indicated on the map. Other reaction conditions: $[C_{NaK}]_0$ = 0.02 M; t_2 = 5 min; and T = 20 °C.

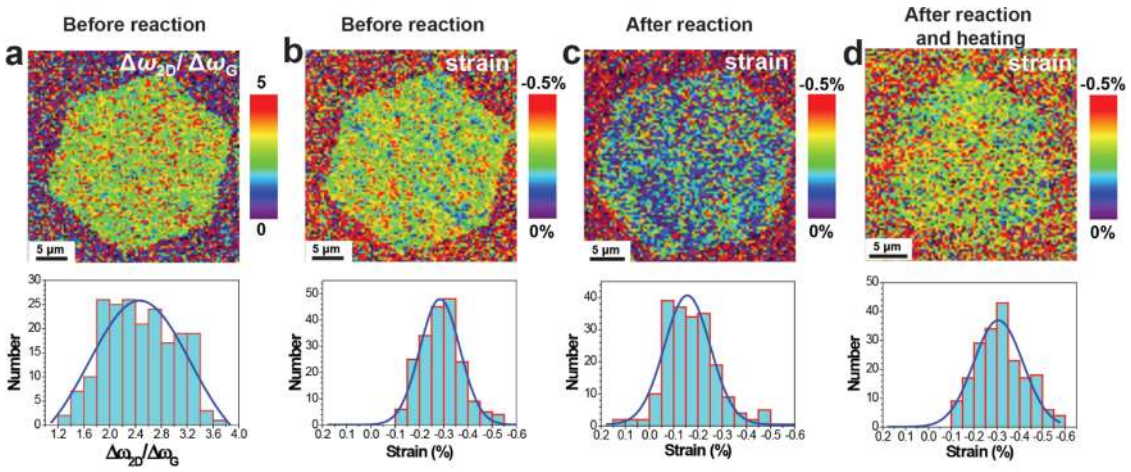

Figure 3. Spatial and statistical analyses of the various parameters for typical 1L islands on Cu(111) after different treatments. (a) $\Delta\omega_{2D}/\Delta\omega_G$ of an unreacted island on Cu(111). (b) Strain of the unreacted island in (a). (c) Strain of another reacted island on Cu(111). (d) Strain of another island on Cu(111) after functionalization, followed by heating at 450 °C in Ar. Statistical analyses were performed using 200 values randomly collected from each map. Electrophilic reagent: iodobenzene; reaction conditions: $[C_{NaK}]_0$ = 0.02 M; t_1 = 5 min; t_2 = 5 min; and T = 20 °C.

significantly higher (10×) (I_D/I_G) value measured for 1L on Cu(111) (I_D/I_G = 2.3) than for those on Cu(100) (I_D/I_G = 0.19) and *p*-Cu (I_D/I_G = 0.13) indicates that graphene on Cu(111) was functionalized to a higher degree. Indeed, the functionalization degree of 1L on Cu(111) was even higher than that for the polycrystalline graphene transferred on SiO_2 (I_D/I_G = 1.1), with the latter reported to be typically showing a relatively high reactivity.[6,20,21] It should be noted that from our previous study, CVD-grown graphene transferred onto SiO_2/Si exhibited a reactivity similar to that of mechanically exfoliated graphene on SiO_2/Si, although the former contains SiO_2 layer hydrates and polymer residues from the requisite transfer processes.[19]

The covalent functionalization of graphene was confirmed from the observation that a near 100% recovery of sp^2-hybridized graphene was achieved by heating at 450 °C under an argon atmosphere (Figure S3). Moreover, we further assessed the reactivity of the four graphenes using bromobenzene, which often displays a lower reactivity than iodobenzene in coupling reactions.[19] The corresponding Raman spectra in Figure 1d show a reactivity sequence similar to that of iodobenzene, although a lower degree of functionalization is observed in all of the graphene samples analyzed. Thus, it can be concluded that the reductive functionalization of graphene is promoted by the Cu(111) substrate.

Reaction Progression and Effect of the Substrate. We independently subjected 1L graphene islands on Cu(111), Cu(100), or *p*-Cu to reductive functionalization to further understand the effect of the substrate on graphene reactivity. Raman mapping was used to monitor the islands over time and the results are shown in Figure 2. Figure 2a shows the evolution of the I_D/I_G map of graphene on Cu(111) during consecutive runs. The first minute of the reaction resulted in relatively uniform functionalization over the whole island and the I_D/I_G ratio was approximately 2 (a typical result obtained

DOI: 10.1021/acs.chemmater.9b01729
Chem. Mater. 2019, 31, 8639−8648

for many such islands on Cu(111) substrates), whereas a slightly higher degree of reduction was measured at the edges. The longer second and third reactions increased the I_D/I_G ratio marginally, indicating that functionalization was nearly complete during the first reaction. In addition, the Raman G and 2D peak frequencies red-shifted from their original positions (Figure S5), consistent with a partial relaxation of the compressive strain during the reaction; this aspect is further described in Figure 3. In contrast, the functionalization of graphene on Cu(100) was nonuniform in all runs as shown in Figure 2b (a typical result for many such islands). Only edges and some "lines" were functionalized to a degree close to graphene on Cu(111). For a 1L island on *p*-Cu, a tenfold larger t_1 was used (Figure 2c), although performing the first reaction for 10 min did not functionalize the island, except at the edges and along some lines, a typical result for many such islands. We note that such lines are not present on the graphene islands on Cu(111). It is likely that these sites were graphene boundaries, cracks, or wrinkles that formed during the CVD growth/cooling process and they readily initiated the functionalization reaction. Functionalization proceeded from the edges and boundaries in the second reaction for 20 min and finally extended to other parts of the island by the end of the third reaction for 50 min (Figure 2c). This "edge-to-interior" reaction suggests that migration of reactants under the graphene layer may play a significant role. A "defect-induced autocatalytic reaction" may also explain the observed reaction process, which proceeds gradually from an edge because graphene may be locally activated by the functionalization of nearby carbon atoms.[39]

The Cu substrate effect was also observed for both continuous graphene films on Cu and graphene islands when using a Li/biphenyl solution (Figures S6 and S7). The influence of the reaction on the morphologies of graphene is seen by atomic force microscopy (AFM) in Figure S8, where a uniform functionalization of graphene only on the Cu(111) foil can be observed. Thus, a Cu(111) foil facilitates the fast and uniform reductive functionalization of epitaxial CVD graphene, which may be desirable for applications where fine control over the degree of functionalization is required. The increased reactivity of graphene on Cu(111) was observed for other reactions, including phenylations that utilize bromobenzene and iodoaniline, respectively. Collectively, these results suggest that Cu substrates may widely affect the chemistry of graphene.

Influence of Compressive Strain. Charge transfer and strain (ε) are two factors that can alter the band energy and thereby cause a shift in the positions of the characteristic Raman peaks of graphene (i.e., ω_G and ω_{2D}). Charge transfer between Cu and graphene is generally weak and does not significantly change the positions of ω_G and ω_{2D} (<2 cm^{-1}),[29] but tensile (positive) and compressive (negative) strains lead, respectively, to red- and blue-shifts of the Raman peaks.[40−45] Moreover, graphene subjected to mechanical strain shows a $\Delta\omega_{2D}/\Delta\omega_G$ of 2.45 ± 0.37,[42] which allows one to distinguish between charge doping and strain effects.[41] From the blue-shifts of the G and 2D bands with respect to ω_G (1582 cm^{-1}) and ω_{2D} (2692 cm^{-1}) values observed for unstrained graphene under 488 nm excitation,[42] and the calculated $\Delta\omega_{2D}/\Delta\omega_G$ value of 2.47 ± 0.54 in Figure 3a, the presence of significant compressive strain on the 1L island on Cu(111) can be confirmed. Indeed, CVD graphene grown on Cu has been reported to experience strain in a manner that is dependent on the substrate crystal lattice.[29] We previously reported that the compressive strain is maintained by the frictional force between the graphene and the underlying Cu(111) substrate.[31] In finding a quantitative relation between the strain and the observed Raman shift, we noted that different correlation coefficients between strain and peak shift ($\partial\omega_G/\partial\varepsilon$ or $\partial\omega_{2D}/\partial\varepsilon$) have been reported in literatures. This difference may arise from various experimental conditions, such as polarization of the laser beam and the orientation of the graphene lattice.[40−45] Here, we used $\partial\omega_G/\partial\varepsilon = -60$ cm^{-1}/% or $\partial\omega_{2D}/\partial\varepsilon = -147$ cm^{-1}/% in our calculation, values that we have taken from reported data on CVD graphene on Cu (no transfer).[29,44] In contrast to these studies using pristine graphene on Cu,[29,44] we have attempted to correlate covalent functionalization to compressive strain. However, since Raman spectral information also includes compressive strain and the 2D band is more dispersive because of defects,[36,37] we have used ω_G to calculate strain in our graphene samples. We found a −0.29 ± 0.08% strain for graphene islands on Cu(111), as shown in Figure 3b.[29] Cu(100) and *p*-Cu produce a lower compression of the graphene than does Cu(111). For example, graphene on Cu(100) has been reported to show a wide distribution of strains from −0.3% (compression) to 0.2% tensile. The islands on Cu(100) and *p*-Cu showed strains of about −0.09% and about −0.05%, respectively, consistent with reported values.[29] The reductive functionalization of a 1L island on Cu(111) was found to partially relax the strain in graphene, the distribution of which is relatively uniform in the strain map in Figure 3c, with an average value of −0.16 ± 0.09%. The removal of grafted groups by heating the functionalized islands in argon at 450 °C resulted in the recovery of strain to −0.31 ± 0.11%, thus providing a way to change the strain in the graphene layer and render it more reactive. We note that some wrinkles survived after the thermal treatment, as shown in Figure S3c−e.

The number of substrate atoms doped in the graphene is relatively small for a copper substrate and depends on the substrate orientation, which is in marked contrast with the high dopant concentrations found when other substrates are used, including Ag, Au, Pt, or Al.[46] It was reported that Cu(111) leads to a shift in the Fermi level of 250 meV, while Cu(100) leads to three distinct doping stages of the Fermi-level shifts: 0, 250, and 350 meV.[29] However, the doping of graphene with Cu induced by the orientation of the Cu surface should not play a dominant role in influencing its reactivity. More importantly, we note that the influence of charge doping between Cu and graphene may be relatively small when compared to the solution of $[K(15\text{-crown-}5)_2]Na$ that was used to reduce the graphene. Since the roughness of the substrate and the quality of graphene are comparable for all three substrates, their respective contributions should be comparable. While it has been reported that graphene on SiO_2/Si can exhibit other types of noncovalent interactions,[47−49] the interaction between graphene and Cu is likely to be dominated by van der Waals forces.[50] As such, the reactant-adsorbing ability of the Cu substrates may not be expected to significantly alter the reactivity displayed by the supported graphene. The enhanced functionalization of graphene on Cu(111) is thus attributed mainly to compressive strain, as supported by the calculations described below, and is consistent with other calculations indicating that compressive strain facilitates chemisorption.[28]

DOI: 10.1021/acs.chemmater.9b01729
Chem. Mater. 2019, 31, 8639−8648

The evolution of the I_D/I_G map in Figure 2 indicates that reductive functionalization probably also involves reactants underneath the graphene rather than exclusively from the "top" surface for islands on Cu(100) or *p*-Cu. For the functionalization of islands on *p*-Cu for 1 h (Figure 2c), if we assume that the interface between graphene and Cu contains reactants, the bottom side of graphene is probably also attended with functional groups. For the functionalization of islands on Cu(111) for 1 min (Figure 2a), we cannot completely exclude the possibility of the reagent moving in the space between the bottom side of the graphene and the substrate; however, the absence of wrinkles of graphene prior to exposure to the reductive conditions suggests that the two-sided reaction would not be favored. Indeed, since the functionalization of continuous films on Cu(111) was also efficient and uniform, we conclude that reaction at the upper surface is dominant (Figure S6). A partial rather than a complete relaxation of compressive strain by functionalization (Figure 3c) and the restoration of strain by heating (Figure 3d) also support preferential reaction at the top surface. Even at low temperatures (−20 °C), the functionalization of the islands on Cu(111) was uniform, although significantly weaker (Figure 5a), which supports the idea that the reaction occurs primarily, or only, on the exposed side of the graphene. Such a reaction preference could be potentially used to prepare two-sided asymmetric functionalized graphene with two faces of different structures.

Theoretical Calculations. We first performed MD simulations to determine the strain state of graphene on a Cu(111) surface (see the MD simulation section in the SI). From the average carbon bond length measured in graphene, we found that a compressive strain of about −0.035% was exerted by the Cu(111) surface. For comparison, a value of −0.3% is shown in Figure 3b. The difference may be due to the different thermal expansion coefficients between the graphene and the underlying metal substrate, which were not included in our calculations.[44,51] Next, DFT was used to calculate how the compressive strain affected the covalent functionalization reaction. As summarized in Figure 4 (and the DFT section in the SI), graphene under various degrees of strain was introduced into a solution of $[K(15\text{-crown-}5)_2]Na$ and iodobenzene. The overall functionalization process was calculated to proceed through a mechanism analogous to those described for radical nucleophilic aromatic substitution ($S_{RN}1$) reactions.[52] During the initial stage, graphene was shown to undergo reduction upon exposure to the $[K(15\text{-crown-}5)_2]Na$. Subsequent electron transfer to iodobenzene resulted in the formation of a phenyl radical species and an iodide byproduct. Finally, coupling between the phenyl group and the graphene proceeded through the transition state shown to form the expected product. The application of strain to the graphene resulted in bond deformation and effectively destabilized the ground state in a manner that facilitated the coupling reaction. In other words, the relative energies of the calculated transition states and products were reduced depending on the compressive strain applied to the graphene. In addition, to investigate the effect of the Cu substrate on the reactivity of graphene, the binding energy of the phenyl group on the graphene flake under increasing compressive strain and in the presence of Cu(111) was also calculated. As shown in Figure S12 and Table S2, compression increased the reactivity displayed by the Cu-supported graphene.

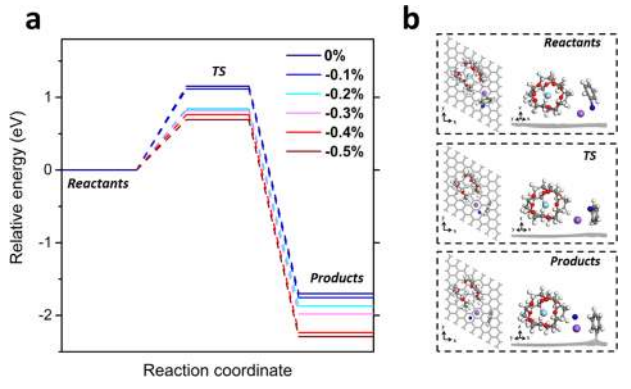

Figure 4. Theoretical study of the reductive functionalization of graphene on Cu(111). (a) Reaction coordinate diagram calculated for the covalent functionalization of reduced graphene (graphenide) with iodobenzene (step 2). (b) Atomic configurations of the corresponding reactants, transition states, and products. White, red, light blue, purple, blue, and gray spheres represent H, O, K, Na, I, and C atoms, respectively. The transparent gray honeycomb network represents a layer of graphene.

Low-Temperature Functionalization and Kinetics. To study the reaction kinetics, T and t_1 were varied in the reductive functionalization of 1L graphene islands on Cu(111). The reaction time (t_2) after the addition of electrophilic reagents does not influence the functionalization (Figure S13).[19] Considering the instability of the heated $[K(15\text{-crown-}5)_2]Na$ solution and the high reaction rate at 20 °C, we used $T \leq 20$ °C to slow down the reaction and first investigated the uniformity of the functionalization at −20 °C. The I_D/I_G map of a functionalized island in Figure 5a shows that the reaction took place over the entire island. However, the average I_D/I_G value of graphene treated at −20 °C is ∼0.7, which is lower than that of the island functionalized at 20 °C as shown in Figure 2a. Figure 5b shows the influence of the size of the graphene island (represented by the total length of the perimeter divided by 6 (P/6)) on the functionalization degree. The similar average I_D/I_G ratios of functionalized islands with P/6 ranging from 10 to 80 μm (at either −20 or 10 °C) indicate that graphene size has no influence on the reductive functionalization. This uniform and size-independent functionalization means that we can use the average I_D/I_G ratio calculated from various graphene islands on Cu(111) to represent the degree of the reaction in our study of the reaction kinetics.

The relationship between I_D/I_G and t_1 for functionalized graphene islands on Cu(111) is plotted in Figure 5c. At −20 °C, I_D/I_G increased gradually with increasing t_1 and reached 1.47 ± 0.49 at t_1 = 20 min. In contrast, at 10 °C, I_D/I_G increased more rapidly with t_1 to reach a maximum of 1.80 ± 0.35 at t_1 = 5 min; further increasing t_1 led to a decrease in I_D/I_G. We also plotted the I_D/I_G of the functionalized islands as a function of T using t_1 = 2, 5, or 10 min. As shown in Figure 5d, when t_1 = 2 or 5 min, I_D/I_G gradually increases with increasing T in the range −30 to 20 °C, whereas, when t_1 = 10 min, I_D/I_G increases with increasing T in the range −30 to 10 °C, with a maximum value of 1.79 ± 0.39 (T = 10 °C). The results shown in Figure 5c,d demonstrate that the degree of functionalization of the graphene islands is influenced by changing the reaction temperature and time. Since the defect density of graphene can be calculated from the I_D/I_G ratios,[35−38] a relationship between functionalization degree and temperature can be derived as

DOI: 10.1021/acs.chemmater.9b01729
Chem. Mater. 2019, 31, 8639−8648

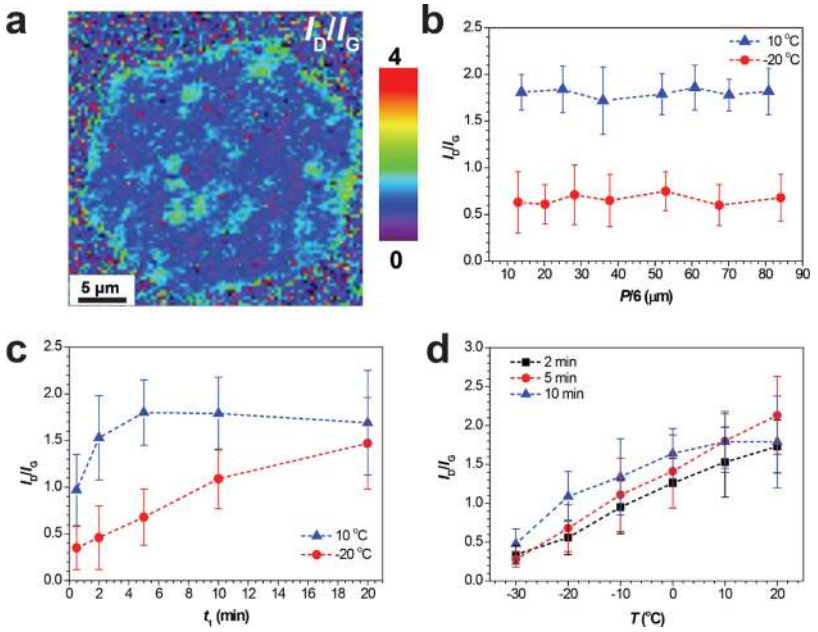

Figure 5. Study of the kinetics of the reductive functionalization of graphene on Cu(111). (a) I_D/I_G map of a 1L graphene island on Cu(111) after "low-temperature" functionalization. Reaction conditions: $[C_{NaK}]_0$ = 0.02 M; t_1 = 5 min; t_2 = 5 min; and T = −20 °C. (b) I_D/I_G ratio of hexagonal islands as a function of graphene size (represented by perimeter/6 (P/6)) after functionalization at −20 or 10 °C. Reaction conditions: $[C_{NaK}]_0$ = 0.02 M; t_1 = 5 min; and t_2 = 5 min. (c) I_D/I_G ratio of islands as a function of t_1. Reaction conditions: $[C_{NaK}]_0$ = 0.02 M, t_2 = 5 min; and T = −20 or 10 °C. (d) I_D/I_G ratio of islands as a function of T. $[C_{NaK}]_0$ = 0.02 M; t_1 = 2, 5, or 10 min; and t_2 = 5 min.

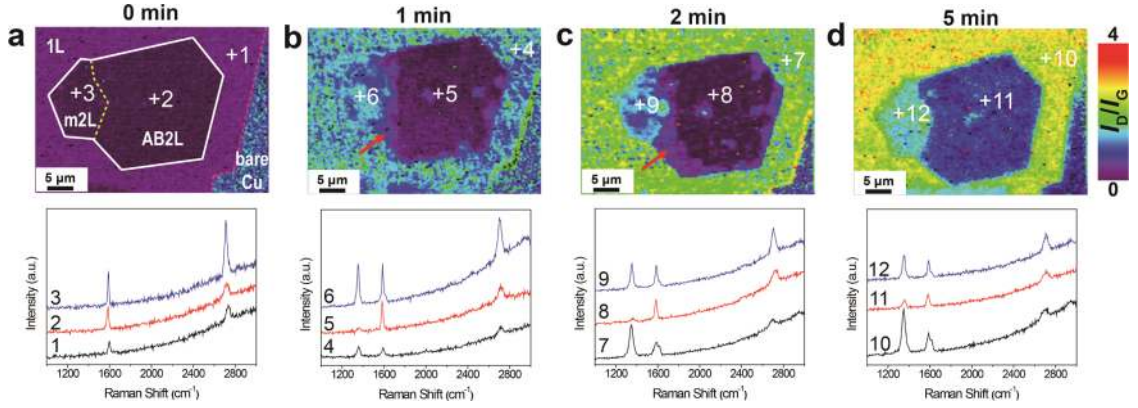

Figure 6. Evolution of Raman spectra recorded for a graphene island containing 1L, AB2L, and m2L regions after successive reductive functionalizations with iodobenzene. (a) Before reaction. (b) After the first reaction (t_1 = 1 min). (c) After the second reaction (t_1 = 2 min). (d) After the third reaction (t_1 = 5 min). Other reaction conditions: $[C_{NaK}]_0$ = 0.02 M; t_2 = 5 min; and T = 20 °C.

shown in Figure S14a. The activation energy for the reductive phenylation of 1L islands was estimated from the resultant kinetics plots to be ca. 20 kJ mol^{-1}.

Functionalization of Bilayer Graphene on Cu(111). We next examined the functionalization of few-layer (in particular, 2L) graphene islands on Cu(111). Our graphene islands were epitaxially grown on Cu(111) and had mostly a hexagonal shape, with their orientation predominantly determined by the substrate lattice. In the case of 2L graphene, we found that ∼70% of the second hexagonal layers (the smaller hexagon) had the same orientation as the first layer (the larger hexagon), indicating epitaxial growth as well as AB-stacking (termed AB2L). Misoriented 2L islands could also be found in these samples, and in this case there was usually a rotation angle of ∼30° between the two layers (termed m2L island). In some cases, the m2L and AB2L regions were connected as shown in Figures 6, S15, and S16.

We found that the blue-shifts in the Raman G and 2D frequencies of few-layer graphene islands were smaller than those of 1L islands on Cu(111), indicating smaller compressive strains in few-layer graphene. Moreover, an AB2L island has a smaller ω_G, but a higher ω_{2D} than an m2L island on Cu(111). It is known that the 2D band of 2L graphene is strongly dependent on the rotation angle between the two layers.[53,54] For example, AB2L has four subpeaks due to the strong coupling between the two layers.[55] In contrast, the 2D band of m2L is a single Lorentzian for rotation angles larger than 13° under 488 nm laser excitation.[53,54] Such a distinction together with the complicated substrate effects makes a comparison of the ω_{2D} of AB2L and m2L less informative. Therefore, we used ω_G to calculate the compressive strain of 2L graphene parallel to the layers using the coefficient $\partial\omega_G/\partial\varepsilon$ to be 60 cm^{-1}/%, as described earlier in this paper. The compressive strains in the AB2L and m2L islands are ∼0.08 and 0.11%, respectively,

DOI: 10.1021/acs.chemmater.9b01729
Chem. Mater. 2019, 31, 8639−8648

suggesting a slightly larger compression for the latter. Indeed, AFM characterization showed that among 1L, AB2L, and m2L islands, the AB2L island had the largest number of step bunches, while the 1L island had the lowest (Figures S15b and S17). In addition, the AB2L island had more pronounced wrinkles than the m2L island (Figure S17). Both step bunching and wrinkles release compression, and as a result, the compressive strain decreases in the order 1L > m2L > AB2L graphene islands.

To compare the reductive functionalization of 2L graphenes, we chose an island consisting of 1L, AB2L, and m2L regions, as shown in Figures 6 and S15. Prior to the functionalization, no D peaks were found for the whole region examined, as shown in Figure 6a. Note that the light purple contrast for the 1L region in Figure 6a is due to the larger intensity ratio resulting from greater noise in the D peak range than for the 2L region. After the first reaction was run for 1 min, we found that m2L was functionalized relatively uniformly to a degree close to the 1L island. In contrast, AB2L was less functionalized, although a small D peak could be seen for the interior regions, suggesting the functionalization of the edge of the AB2L region was more severe. The second reaction slightly increased the functionalization of both 1L and m2L regions, and the functionalization of the AB2L region proceeded from the edge. The third reaction for 5 min led to the uniform functionalization of all graphenes, and the functionalization of AB2L covered its whole area. The sequence of reactivity 1L > m2L > AB2L is the same as that observed for compressive strain. Note that the I_D/I_G ratio is affected by the number and stacking order of the graphene layers, potentially because the defects in one layer can scatter phonons in a neighboring layer.[56] As such, the quantification of defect densities in bilayer graphene using Raman spectroscopy is challenging, although qualitative assessments of relative reactivity may be possible. Changes in the strain maps in each stage (Figure S16) further show the release of compressive strain. The reaction process for the AB2L region in Figure 6 is similar to that for bilayer graphene in our previous study,[19] suggesting that intercalation of reactants between the two layers is dominant. The intercalation process of the AB2L region on Cu(111) is faster than that for mechanically exfoliated bilayer flakes on SiO_2/Si,[19] which is likely due to the different substrate. However, reaction on the top surface of AB2L on Cu(111) cannot be excluded since a weak D peak is observed everywhere on the sample. The examination of individual AB2L and m2L islands (Figures S17−S20) gives further information on the differences in reactivity between the two kinds of graphene in reductive functionalization. It has been reported that misoriented bilayer graphene has a higher reactivity than AB-stacked graphene, and this has been said to be due to the different Fermi levels of the two bilayers.[10,15] We speculate that on Cu(111), the intrinsic reactivity and compressive strain also contribute to the higher degree of functionalization of m2L when compared to that of AB2L islands.[57]

CONCLUSIONS

Epitaxial graphene (single-layer islands and continuous films) grown on Cu(111) experiences significant biaxial compressive strain in a manner that facilitates reductive reactions, leading to fast and uniform functionalization, as illustrated by Raman mapping. In comparison, graphene grown on Cu(100) and polycrystalline Cu undergoes slow and nonuniform functionalization that proceeds from the edge to the interior. The activation of graphene on a Cu(111) foil was attributed to compressive strain. Functionalization relaxed this compression, while heating to a temperature that promoted defunctionalization restored compression to almost its original value. The kinetics was investigated for a set of reactions performed below room temperature, and an activation energy of around 20 kJ mol^{-1} was measured for the functionalization of reduced graphene using iodobenzene. Molecular dynamics and density functional theory calculations were used to elucidate the mechanism of the reaction and the effect of compression. A noticeably higher reactivity was observed for misoriented bilayer graphene than for AB-stacked bilayer graphene, which was attributed to the difference in their energies and compressive strains. This study describes the chemistry of graphene grown on metal substrates, demonstrates how surface reactivity may be kinetically controlled, and shows that such chemical reactions can be reversed by heating, which defunctionalizes the graphene and changes the level of compressive strain in it.

EXPERIMENTAL METHODS

Graphene Preparation. *Graphene on Cu(111).* A commercial polycrystalline Cu foil (99.99%, thickness = 80 μm, Nilaco Co., Japan) was heated in a tube furnace at 1050 °C and 760 Torr under a mixed H_2/Ar flow (10 sccm for each) for 12 h to prepare a single-crystal Cu(111) foil.[34] The foil was electrochemically polished in an electrolyte containing 500 mL H_3PO_4 (14.7 M), 250 mL ethanol, 50 mL isopropyl alcohol, and 5 g urea under a constant voltage (>2 V) for 30 min, washed with deionized water and acetone, and dried under flowing N_2.

For the CVD growth of graphene, the Cu(111) foil was heated in a tube furnace at 1075 °C and 760 Torr under a mixed H_2 (500 sccm) and Ar (1000 sccm) flow for 2 h. The H_2 flow was then reduced to 55 sccm, and CH_4 (0.1% in Ar, prepared using a homemade premixing system) was introduced at a flow rate of 40 sccm for a given time to obtain epitaxial growth of graphene. The graphene samples with different sizes and numbers of layers grown on Cu(111), used in this study, were obtained by controlling the exposure time to CH_4.

Graphene on Cu(100). A commercial polycrystalline Cu foil (99.99%, thickness = 80 μm, Chinalco Co., China) was used for the preparation of the Cu(100) substrates by thermal heating.[34] The CVD growth of graphene was performed in a tube furnace at 1060 °C and 760 Torr under CH_4 (0.1% in Ar using a homemade premixing system, 34 sccm), H_2 (36 sccm), and Ar (200 sccm) flows for around 2 h.

Graphene on Polycrystalline Cu. To grow graphene on polycrystalline Cu, a Cu foil (99.8%, thickness = 25 μm, Alfa Aesar) was used. Prior to graphene growth, the foil was immersed in acetic acid for 30 min and dried under a N_2 flow. Graphene was nonepitaxially grown on the Cu foil at 1035 °C under H_2 (25 sccm) and CH_4 (2 sccm) flow for a given time at a pressure of 0.3 Torr. Continuous or partial coverage of monolayer graphene was obtained by controlling the time of exposure to CH_4.

Graphene on SiO_2/Si. Continuous single-layer graphene grown on a polycrystalline Cu foil (99.8%, thickness = 25 μm, Alfa Aesar) was transferred onto SiO_2 (300 nm)/Si using the PMMA transfer method.

Functionalization of Graphene. *Functionalization at Room Temperature.* The two-step functionalization of graphene at room temperature (20 ± 1 °C) was performed inside an argon glovebox. A sodium−potassium alloy (NaK, liquid, 1:1 atom ratio) was prepared by combining sodium (99.95%, Sigma-Aldrich) and potassium (99.95%, Sigma-Aldrich), and was stored in a glovebox. In a glass Petri dish, 15-crown-5 (98%, 88 mg, 0.4 mmol, Sigma-Aldrich) was dissolved in anhydrous THF (5 mL). A suspension of the NaK (12.4 mg, 0.2 mmol) in THF (5 mL) was added to the solution of 15-crown-5, under stirring, using a glass-coated magnetic bar. When using 18-crown-6 (98%, Sigma-Aldrich) or cryptand 222 (98%,

DOI: 10.1021/acs.chemmater.9b01729
Chem. Mater. 2019, 31, 8639−8648

Sigma-Aldrich), the stoichiometric ratio of the macrocyclic host to NaK was 1:1. For simplicity, we used the concentration of the NaK ($[C_{NaK}]_0$) to describe the concentration of the reductive complex solution. The mixture became dark blue within ~1 min due to the formation of the reductive K(15-crown-5)$_2$Na solution; the solution (0.02 M) was further stirred for 10−20 min. A graphene sample was then immersed in the solution for a given reaction time in the first step (t_1), followed by the dropwise addition of an aryl or alkyl halide (1 mmol in 5 mL THF). The graphene sample was kept in the solution for a given reaction time in a second step (t_2). After the reaction, the graphene sample was washed with THF inside the glovebox and then removed. The sample was then washed with methanol and acetone and dried under flowing N_2.

Functionalization at Low Temperatures. Functionalization of the graphene at low temperatures was carried out in a three-neck round-bottom flask inside a fume hood. A homemade Cu clamp piercing a rubber stopper was used to hold the graphene on the substrates. The flask equipped with the clamp and a glass-coated stirrer was sealed with a stopper and filled with argon gas. The flask was then cooled to the target temperature using either a water bath (≥0 °C) or an acetone/dry ice bath (<0 °C). The temperature was controlled to within ±1 °C. A solution of K(15-crown-5)$_2$Na (0.02 M, 30 mL) was prepared in a single-neck flask inside an argon glovebox, sealed with a rubber stopper, and removed from the glovebox. The solution was then transferred to the three-neck flask using a syringe and stirred for 5 min. The graphene sample was then immersed in the K(15-crown-5)$_2$Na solution for a given time (t_1), followed by the dropwise addition of iodobenzene (3 mmol in 5 mL THF) by a syringe. The graphene sample was kept in the solution for another 5 min in a second step (t_2), taken out of the flask, washed, and dried as described earlier.

Characterization. Raman spectroscopy studies were performed using a Raman spectrometer (WITec GmbH) using 488 nm laser excitation under low power (<2 mW) at room temperature. AFM images were acquired with a Bruker Dimension Icon system. Scanning electron microscopy (SEM) and EBSD images were obtained using an FEI Verios 460 SEM system.

Theoretical Calculations. All-atom MD simulation was performed with the COMPASS II force field[58] to describe the interaction between the graphene island and the Cu substrate (i.e., (111) surface). DFT calculations were used to elucidate the effect of compressive strain on the covalent functionalization using a DMol^3 program.[59,60] More details of the calculations are presented in the Supporting Information.

■ ASSOCIATED CONTENT

Supporting Information

The Supporting Information is available free of charge on the ACS Publications website at DOI: 10.1021/acs.chemmater.9b01729.

SEM images, EBSD images, Raman spectra, AFM images, and detailed information about MD, DFT calculations, and kinetics studies (PDF)

■ AUTHOR INFORMATION

Corresponding Authors

*E-mail: zhangx@bjut.edu.cn (X.Z.).
*E-mail: bielawski@unist.ac.kr (C.W.B.).
*E-mail: rsruoff@ibs.re.kr, ruofflab@gmail.com (R.S.R.).

ORCID

Xu Zhang: 0000-0001-7320-4360
Da Luo: 0000-0002-9128-6782
Hanyang Zhang: 0000-0002-6945-2959
Mandakini Biswal: 0000-0002-1295-1095
Yi Jiang: 0000-0003-1080-5884
Yuan Huang: 0000-0002-7005-1319
Sang Kyu Kwak: 0000-0002-0332-1534
Christopher W. Bielawski: 0000-0002-0520-1982

Present Address

#College of Materials Science and Engineering, Key Laboratory of Advanced Functional Materials, Education Ministry of China, Beijing University of Technology, Beijing 100124, P. R. China (X.Z.)

Notes

The authors declare no competing financial interest.

■ ACKNOWLEDGMENTS

This work was supported by IBS-R019-D1 and by the Outstanding Research Fund (1.180066.01) of Ulsan National Institute of Science & Technology. C.W.B. is grateful for the support of the BK21 Plus Program funded by the Ministry of Education and the National Research Foundation of Korea. X.Z. acknowledges the financial support from the National Natural Science Foundation of China (No. 51802009), and is grateful to Prof. Feng Ding for the discussions about reaction pathways.

■ REFERENCES

(1) Georgakilas, V.; Otyepka, M.; Bourlinos, A. B.; Chandra, V.; Kim, N.; Kemp, K. C.; Hobza, P.; Zboril, R.; Kim, K. S. Functionalization of Graphene: Covalent and Non-Covalent Approaches, Derivatives and Applications. *Chem. Rev.* **2012**, *112*, 6156−6214.

(2) Eigler, S.; Hirsch, A. Chemistry with Graphene and Graphene Oxide-Challenges for Synthetic Chemists. *Angew. Chem., Int. Ed.* **2014**, *53*, 7720−7738.

(3) Criado, A.; Melchionna, M.; Marchesan, S.; Prato, M. The Covalent Functionalization of Graphene on Substrates. *Angew. Chem., Int. Ed.* **2015**, *54*, 10734−10750.

(4) Sinitskii, A.; Dimiev, A.; Corley, D. A.; Fursina, A. A.; Kosynkin, D. V.; Tour, J. M. Kinetics of Diazonium Functionalization of Chemically Converted Graphene Nanoribbons. *ACS Nano* **2010**, *4*, 1949−1954.

(5) Sharma, R.; Baik, J. H.; Perera, C. J.; Strano, M. S. Anomalously Large Reactivity of Single Graphene Layers and Edges toward Electron Transfer Chemistries. *Nano Lett.* **2010**, *10*, 398−405.

(6) Wang, Q. H.; Jin, Z.; Kim, K. K.; Hilmer, A. J.; Paulus, G. L. C.; Shih, C. J.; Ham, M. H.; Sanchez-Yamagishi, J. D.; Watanabe, K.; Taniguchi, T.; Kong, J.; Jarillo-Herrero, P.; Strano, M. S. Understanding and controlling the substrate effect on graphene electron-transfer chemistry via reactivity imprint lithography. *Nat. Chem.* **2012**, *4*, 724−732.

(7) Wang, Q. H.; Shih, C. J.; Paulus, G. L. C.; Strano, M. S. Evolution of Physical and Electronic Structures of Bilayer Graphene upon Chemical Functionalization. *J. Am. Chem. Soc.* **2013**, *135*, 18866−18875.

(8) Bissett, M. A.; Konabe, S.; Okada, S.; Tsuji, M.; Ago, H. Enhanced Chemical Reactivity of Graphene Induced by Mechanical Strain. *ACS Nano* **2013**, *7*, 10335−10343.

(9) Wu, Q. Z.; Wu, Y. P.; Hao, Y. F.; Geng, J. X.; Charlton, M.; Chen, S. S.; Ren, Y. J.; Ji, H. X.; Li, H. F.; Boukhvalov, D. W.; Piner, R. D.; Bielawski, C. W.; Ruoff, R. S. Selective surface functionalization at regions of high local curvature in graphene. *Chem. Commun.* **2013**, *49*, 677−679.

(10) Ding, Y.; Peng, Q.; Gan, L.; Wu, R. Z.; Ou, X. W.; Zhang, Q. C.; Luo, Z. T. Stacking-Mode-Induced Reactivity Enhancement for Twisted Bilayer Graphene. *Chem. Mater.* **2016**, *28*, 1034−1039.

(11) Zhou, L.; Liao, L.; Wang, J. Y.; Yu, J. W.; Li, D. H.; Xie, Q.; Liu, Z. R.; Yang, Y. L.; Guo, X. F.; Liu, Z. F. Substrate-Induced Graphene Chemistry for 2D Superlattices with Tunable Periodicities. *Adv. Mater.* **2016**, *28*, 2148−2154.

DOI: 10.1021/acs.chemmater.9b01729
Chem. Mater. 2019, 31, 8639−8648

(12) Sarkar, S.; Bekyarova, E.; Niyogi, S.; Haddon, R. C. Diels-Alder Chemistry of Graphite and Graphene: Graphene as Diene and Dienophile. *J. Am. Chem. Soc.* **2011**, *133*, 3324−3327.
(13) Li, J.; Li, M.; Zhou, L. L.; Lang, S. Y.; Lu, H. Y.; Wang, D.; Chen, C. F.; Wan, L. J. Click and Patterned Functionalization of Graphene by Diels-Alder Reaction. *J. Am. Chem. Soc.* **2016**, *138*, 7448−7451.
(14) Liu, H. T.; Ryu, S. M.; Chen, Z. Y.; Steigerwald, M. L.; Nuckolls, C.; Brus, L. E. Photochemical Reactivity of Graphene. *J. Am. Chem. Soc.* **2009**, *131*, 17099−17101.
(15) Liao, L.; Wang, H.; Peng, H.; Yin, J. B.; Koh, A. L.; Chen, Y. L.; Xie, Q.; Peng, H. L.; Liu, Z. F. van Hove Singularity Enhanced Photochemical Reactivity of Twisted Bilayer Graphene. *Nano Lett.* **2015**, *15*, 5585−5589.
(16) Englert, J. M.; Dotzer, C.; Yang, G. A.; Schmid, M.; Papp, C.; Gottfried, J. M.; Steinruck, H. P.; Spiecker, E.; Hauke, F.; Hirsch, A. Covalent bulk functionalization of graphene. *Nat. Chem.* **2011**, *3*, 279−286.
(17) Englert, J. M.; Vecera, P.; Knirsch, K. C.; Schafer, R. A.; Hauke, F.; Hirsch, A. Scanning-Raman-Microscopy for the Statistical Analysis of Covalently Functionalized Graphene. *ACS Nano* **2013**, *7*, 5472−5482.
(18) Schafer, R. A.; Weber, K.; Kolesnik-Gray, M.; Hauke, F.; Krstic, V.; Meyer, B.; Hirsch, A. Substrate-Modulated Reductive Graphene Functionalization. *Angew. Chem., Int. Ed.* **2016**, *55*, 14858−14862.
(19) Biswal, M.; Zhang, X.; Schilter, D.; Lee, T. K.; Hwang, D. Y.; Saxena, M.; Lee, S. H.; Chen, S. S.; Kwak, S. K.; Bielawski, C. W.; Bacsa, W. S.; Ruoff, R. S. Sodide and Organic Halides Effect Covalent Functionalization of Single-Layer and Bilayer Graphene. *J. Am. Chem. Soc.* **2017**, *139*, 4202−4210.
(20) Yamamoto, M.; Einstein, T. L.; Fuhrer, M. S.; Cullen, W. G. Charge Inhomogeneity Determines Oxidative Reactivity of Graphene on Substrates. *ACS Nano* **2012**, *6*, 8335−8341.
(21) Lee, J. H.; Avsar, A.; Jung, J.; Tan, J. Y.; Watanabe, K.; Taniguchi, T.; Natarajan, S.; Eda, G.; Adam, S.; Neto, A. H. C.; Ozyilmaz, B. van der Waals Force: A Dominant Factor for Reactivity of Graphene. *Nano Lett.* **2015**, *15*, 319−325.
(22) Koehler, F. M.; Jacobsen, A.; Ensslin, K.; Stampfer, C.; Stark, W. J. Selective Chemical Modification of Graphene Surfaces: Distinction Between Single- and Bilayer Graphene. *Small* **2010**, *6*, 1125−1130.
(23) Robinson, J. T.; Burgess, J. S.; Junkermeier, C. E.; Badescu, S. C.; Reinecke, T. L.; Perkins, F. K.; Zalalutdniov, M. K.; Baldwin, J. W.; Culbertson, J. C.; Sheehan, P. E.; Snow, E. S. Properties of Fluorinated Graphene Films. *Nano Lett.* **2010**, *10*, 3001−3005.
(24) Gao, G. D.; Liu, D. D.; Tang, S. C.; Huang, C.; He, M. C.; Guo, Y.; Sun, X. D.; Gao, B. Heat-Initiated Chemical Functionalization of Graphene. *Sci. Rep.* **2016**, *6*, No. 20034.
(25) Plšek, J.; Kovaricek, P.; Vales, V.; Kalbac, M. Tuning the Reactivity of Graphene by Surface Phase Orientation. *Chem. - Eur. J.* **2017**, *23*, 1839−1845.
(26) Li, X.; Cai, W. W.; An, J. H.; Kim, S.; Nah, J.; Yang, D. X.; Piner, R.; Velamakanni, A.; Jung, I.; Tutuc, E.; Banerjee, S. K.; Colombo, L.; Ruoff, R. S. Large-Area Synthesis of High-Quality and Uniform Graphene Films on Copper Foils. *Science* **2009**, *324*, 1312−1314.
(27) Qiu, B.; Zhang, M. H.; Wu, L. J.; Wang, J.; Xia, Y. G.; Qian, D. N.; Liu, H. D.; Hy, S.; Chen, Y.; An, K.; Zhu, Y. M.; Liu, Z. P.; Meng, Y. S. Gas-solid interfacial modification of oxygen activity in layered oxide cathodes for lithium-ion batteries. *Nat. Commun.* **2016**, *7*, No. 12108.
(28) Yi, D.; Luo, D.; Wang, Z. J.; Dong, J. C.; Zhang, X.; Willinger, M. G.; Ruoff, R. S.; Ding, F. What Drives Metal-Surface Step Bunching in Graphene Chemical Vapor Deposition? *Phys. Rev. Lett.* **2018**, *120*, No. 246101.
(29) Frank, O.; Vejpravova, J.; Holy, V.; Kavan, L.; Kalbac, M. Interaction between graphene and copper substrate: The role of lattice orientation. *Carbon* **2014**, *68*, 440−451.
(30) Kang, J. H.; Moon, J.; Kim, D. J.; Kim, Y.; Jo, I.; Jeon, C.; Lee, J.; Hong, B. H. Strain Relaxation of Graphene Layers by Cu Surface Roughening. *Nano Lett.* **2016**, *16*, 5993−5998.
(31) Li, B. W.; Luo, D.; Zhu, L. Y.; Zhang, X.; Jin, S. H.; Huang, M.; Ding, F.; Ruoff, R. S. Orientation-Dependent Strain Relaxation and Chemical Functionalization of Graphene on a Cu(111) Foil. *Adv. Mater.* **2018**, *30*, No. 1706504.
(32) Grobelny, Z.; Stolarzewicz, A.; Sokol, M.; Grobelny, J.; Janeczek, H. Enhanced Stability of Potassium Solutions in Tetrahydrofuran Containing 15-Crown-5. *J. Phys. Chem. A.* **1992**, *96*, 5193−5196.
(33) Stolarzewicz, A.; Grobelny, Z.; Grobelny, J. Characterization of potassium and sodium-potassium alloy solutions containing metal anions and complexed cations by means of NMR and ESR techniques. *Spectrochim. Acta, Part A* **2000**, *56*, 1257−1265.
(34) Jin, S.; Huang, M.; Kwon, Y.; Zhang, L. N.; Li, B. W.; Oh, S.; Dong, J. C.; Luo, D.; Biswal, M.; Cunning, B. V.; Bakharev, P. V.; Moon, I.; Yoo, W. J.; Camacho-Mojica, D. C.; Kim, Y. J.; Lee, S. H.; Wang, B.; Seong, W. K.; Saxena, M.; Ding, F.; Shin, H. J.; Ruoff, R. S. Colossal grain growth yields single-crystal metal foils by contact-free annealing. *Science* **2018**, *362*, 1021−1025.
(35) Ferrari, A. C.; Robertson, J. Interpretation of Raman spectra of disordered and amorphous carbon. *Phys. Rev. B* **2000**, *61*, 14095−14107.
(36) Ferreira, E. H. M.; Moutinho, M. V. O.; Stavale, F.; Lucchese, M. M.; Capaz, R. B.; Achete, C. A.; Jorio, A. Evolution of the Raman spectra from single-, few-, and many-layer graphene with increasing disorder. *Phys. Rev. B* **2010**, *82*, No. 125429.
(37) Cançado, L. G.; Jorio, A.; Ferreira, E. H. M.; Stavale, F.; Achete, C. A.; Capaz, R. B.; Moutinho, M. V. O.; Lombardo, A.; Kulmala, T. S.; Ferrari, A. C. Quantifying Defects in Graphene via Raman Spectroscopy at Different Excitation Energies. *Nano Lett.* **2011**, *11*, 3190−3196.
(38) Lucchese, M. M.; Stavale, F.; Ferreira, E. H. M.; Vilani, C.; Moutinho, M. V. O.; Capaz, R. B.; Achete, C. A.; Jorio, A. Quantifying ion-induced defects and Raman relaxation length in graphene. *Carbon* **2010**, *48*, 1592−1597.
(39) Liao, L.; Song, Z. H.; Zhou, Y.; Wang, H.; Xie, Q.; Peng, H. L.; Liu, Z. F. Photoinduced Methylation of Graphene. *Small* **2013**, *9*, 1348−1352.
(40) Mohiuddin, T. M. G.; Lombardo, A.; Nair, R. R.; Bonetti, A.; Savini, G.; Jalil, R.; Bonini, N.; Basko, D. M.; Galiotis, C.; Marzari, N.; Novoselov, K. S.; Geim, A. K.; Ferrari, A. C. Uniaxial strain in graphene by Raman spectroscopy: G peak splitting, Gruneisen parameters, and sample orientation. *Phys. Rev. B* **2009**, *79*, No. 205433.
(41) Lee, J. E.; Ahn, G.; Shim, J.; Lee, Y. S.; Ryu, S. Optical separation of mechanical strain from charge doping in graphene. *Nat. Commun.* **2012**, *3*, No. 1024.
(42) Zabel, J.; Nair, R. R.; Ott, A.; Georgiou, T.; Geim, A. K.; Novoselov, K. S.; Casiraghi, C. Raman Spectroscopy of Graphene and Bilayer under Biaxial Strain: Bubbles and Balloons. *Nano Lett.* **2012**, *12*, 617−621.
(43) Ding, F.; Ji, H. X.; Chen, Y. H.; Herklotz, A.; Dorr, K.; Mei, Y. F.; Rastelli, A.; Schmidt, O. G. Stretchable Graphene: A Close Look at Fundamental Parameters through Biaxial Straining. *Nano Lett.* **2010**, *10*, 3453−3458.
(44) Yu, V.; Whiteway, E.; Maassen, J.; Hilke, M. Raman spectroscopy of the internal strain of a graphene layer grown on copper tuned by chemical vapor deposition. *Phys. Rev. B* **2011**, *84*, No. 205407.
(45) Pan, W.; Xiao, J. L.; Zhu, J. W.; Yu, C. X.; Zhang, G.; Ni, Z. H.; Watanabe, K.; Taniguchi, T.; Shi, Y.; Wang, X. R. Biaxial Compressive Strain Engineering in Graphene/Boron Nitride Heterostructures. *Sci. Rep.* **2012**, *2*, No. 893.
(46) Khomyakov, P. A.; Giovannetti, G.; Rusu, P. C.; Brocks, G.; van den Brink, J.; Kelly, P. J. First-principles study of the interaction and charge transfer between graphene and metals. *Phys. Rev. B* **2009**, *79*, No. 195425.

DOI: 10.1021/acs.chemmater.9b01729
Chem. Mater. 2019, 31, 8639−8648

(47) Na, S. R.; Suk, J. W.; Ruoff, R. S.; Huang, R.; Liechti, K. M. Ultra Long-Range Interactions between Large Area Graphene and Silicon. *ACS Nano* **2014**, *8*, 11234−11242.
(48) Ambrosetti, A.; Silvestrelli, P. L. Faraday-like Screening by Two-Dimensional Nanomaterials: A Scale-Dependent Tunable Effect. *J. Phys. Chem. Lett.* **2019**, *10*, 2044−2050.
(49) Ambrosetti, A.; Silvestrelli, P. L. Hidden by graphene - Towards effective screening of interface van der Waals interactions via monolayer coating. *Carbon* **2018**, *139*, 486−491.
(50) Batzill, M. The surface science of graphene: Metal interfaces, CVD synthesis, nanoribbons, chemical modifications, and defects. *Surf. Sci. Rep.* **2012**, *67*, 83−115.
(51) N'Diaye, A. T.; van Gastel, R.; Martinez-Galera, A. J.; Coraux, J.; Hattab, H.; Wall, D.; zu Heringdorf, F. J. M.; Horn-von Hoegen, M.; Gomez-Rodriguez, J. M.; Poelsema, B.; Busse, C.; Michely, T. In situ observation of stress relaxation in epitaxial graphene. *New. J. Phys.* **2009**, *11*, No. 113056.
(52) Rossi, R. A.; Pierini, A. B.; Penenory, A. B. Nucleophilic substitution reactions by electron transfer. *Chem. Rev.* **2003**, *103*, 71−167.
(53) Kim, K.; Coh, S.; Tan, L. Z.; Regan, W.; Yuk, J. M.; Chatterjee, E.; Crommie, M. F.; Cohen, M. L.; Louie, S. G.; Zettl, A. Raman Spectroscopy Study of Rotated Double-Layer Graphene: Misorientation-Angle Dependence of Electronic Structure. *Phys. Rev. Lett.* **2012**, *108*, No. 246103.
(54) Carozo, V.; Almeida, C. M.; Fragneaud, B.; Bede, P. M.; Moutinho, M. V. O.; Ribeiro-Soares, J.; Andrade, N. F.; Souza, A. G.; Matos, M. J. S.; Wang, B.; Terrones, M.; Capaz, R. B.; Jorio, A.; Achete, C. A.; Cancado, L. G. Resonance effects on the Raman spectra of graphene superlattices. *Phys. Rev. B* **2013**, *88*, No. 085401.
(55) Ferrari, A. C.; Meyer, J. C.; Scardaci, V.; Casiraghi, C.; Lazzeri, M.; Mauri, F.; Piscanec, S.; Jiang, D.; Novoselov, K. S.; Roth, S.; Geim, A. K. Raman spectrum of graphene and graphene layers. *Phys. Rev. Lett.* **2006**, *97*, No. 187401.
(56) Yang, C.; Zhang, C.; Huo, Y. Y.; Jiang, S. Z.; Qiu, H. W.; Xu, Y. Y.; Li, X. H.; Man, B. Y. Shell-isolated graphene@Cu nanoparticles on graphene@Cu substrates for the application in SERS. *Carbon* **2016**, *98*, 526−533.
(57) The composition and structure of the macrocyclic ligand was also found to influence the reductive functionalization and thus provides a means to finely tune the reaction (see Figure S21).
(58) Sun, H.; Jin, Z.; Yang, C. W.; Akkermans, R. L. C.; Robertson, S. H.; Spenley, N. A.; Miller, S.; Todd, S. M. COMPASS II: extended coverage for polymer and drug-like molecule databases. *J. Mol. Model.* **2016**, *22*, 47.
(59) Delley, B. An All-Electron Numerical-Method for Solving the Local Density Functional for Polyatomic-Molecules. *J. Chem. Phys.* **1990**, *92*, 508−517.
(60) Delley, B. From molecules to solids with the DMol(3) approach. *J. Chem. Phys.* **2000**, *113*, 7756−7764.

DOI: 10.1021/acs.chemmater.9b01729
Chem. Mater. 2019, 31, 8639−8648